Journal of Fluids and Structures (2002) **16**(2), 229–245
doi:10.1006/jfls.2001.0418, available online at http://www.idealibrary.com on IDEAL®

TWO-DIMENSIONAL VORTEX-INDUCED VIBRATION OF CABLE SUSPENSIONS

W.-J. Kim and N. C. Perkins

Department of Mechanical Engineering, University of Michigan
Ann Arbor, MI 48109, U.S.A.

(Received 25 July 2000, and in final form 9 August 2001)

Resonant responses of suspended elastic cables driven by a steady current are investigated. Phenomenological fluid force models for alternate vortex-shedding are coupled with the nonlinear partial differential equations of cable motion. Decoupled cross-flow and in-line vortex-induced vibrations (VIV) are examined first using linearized and nonlinear cable models. The linearized cable model predicts well the basic characteristics of VIV and the nonlinear cable model captures the hysteresis often observed in experiments. Next, coupled cross-flow and in-line vibrations are evaluated by considering two principal coupling mechanisms: (i) cable structural nonlinearities, and (ii) coupled fluid lift and drag. Attention is focused on a "worst-case" resonant response where the natural frequencies for cable modes in the cross-flow and in-line directions are in the same 1 : 2 ratio as the excitation frequencies associated with lift and drag. The inclusion of cable structural nonlinearities alone leads to coupled responses that differ qualitatively (i.e., in number and stability of periodic motions) when compared to those of the decoupled model. The inclusion of coupled fluid lift and drag produces non-planar "figure eight" motions of the cable cross-section that exhibit similar characteristics to those previously measured on spring supported cylinders.

1. INTRODUCTION

Structures subject to a flowing fluid may experience sustained vibrations under certain flow conditions due to the transfer of energy from the fluid to the structure. Such flow-induced vibrations exist in diverse engineering applications including heat exchanger tubes, airplane wings, electric power lines, long span bridges, and underwater risers and cables. A common flow-induced vibration derives from the periodic vortex shedding from a structure. For cables, this vortex-induced vibration (VIV) may promote fatigue and significantly degrade the service life and performance of any attached structure or instrument.

While many studies have focused on VIV, this phenomenon is still far from fully understood due largely to the significant nonlinear mechanisms controlling the fluid and the structure. Following Strouhal's discovery of the relationship between the vortex-shedding frequency and the mean fluid velocity, numerous experimental, analytical and numerical studies have revealed the underlying characteristics of VIV. Extensive reviews are available in Sarpkaya (1979), Griffin *et al.* (1982), Parkinson (1989), and Pantazopoulos (1994). Experiments show that the frequency of (alternate) vortex shedding predicted by the Strouhal relation $f_s = \mathrm{St}\, V/D$ (where V is the mean flow velocity, St is the Strouhal number, and D is the diameter of the structure) locks onto the natural frequency of a flexible (or flexibly mounted) structure. This phenomenon, called *lock-in*, *synchronization or wake-capture*, leads to a resonant vibration of the structure. Lock-in can increase the vortex strength, cross-flow forces (lift), correlation length, and mean drag.

0889–9746/02/020229 + 17 $35.00/0

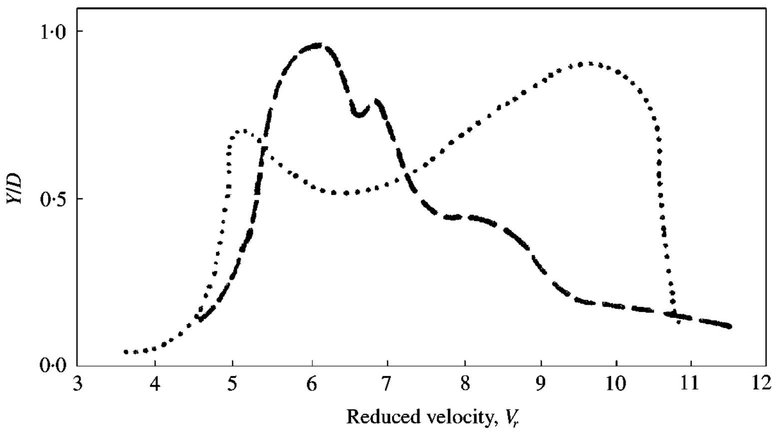

Figure 1. Amplitude of cross-flow vibration of the spring-supported rigid cylinder when the in-line response is eliminated (- - - -) and when it is partially restrained by elastic supports (· · · · · ·). Reproduced from Moe *et al.* (1994).

The majority of studies concentrate on the cross-flow (lift direction) response of cylindrical structures (rigid or flexibly mounted cylinders, pipes, cables, etc.) that are either harmonically driven or self-excited by the fluid flow. Nevertheless, in-line motions may also coexist though they are often an order of magnitude smaller than cross-flow motions. A considerable number of analytical and numerical models have been proposed to evaluate cross-flow response including (i) wake-oscillator models (Hartlen & Currie 1970; Skop & Griffin 1973; Iwan & Blevins, 1974), (ii) single-degree-of-freedom models (Staubli 1983; Goswami *et al*., 1993), (iii) random vibration models (Blevins & Burton 1976; Kennedy & Vandiver 1979), and (iv) numerical models based on the Navier–Stokes equation (Lu & Dalton 1996; Blackburn & Henderson 1996).

By contrast, only a few analytical models have been proposed for the in-line response of structures (Currie & Turnbull 1987; Naudascher 1987). As revealed in experiments (Bishop & Hassan 1964), the frequency of in-line vibration is twice that of cross-flow vibration. Unlike the cross-flow VIV, in-line vibration possesses two resonances (Currie & Turnbull 1987; Naudascher 1987). The first resonance originates from symmetric vortex shedding and the second from alternate vortex shedding.

Even fewer studies consider the possible coupling of the cross-flow and in-line responses as reported in several experiments (Alexander 1981; Wu 1989; Moe *et al.* 1994). For example, Figure 1 illustrates experimental results by Moe *et al.* (1994) for a spring supported rigid cylinder subject to a uniform flow. Here, Y denotes the amplitude of the vibration and $V_r = V/Df_n$ is the reduced velocity in which f_n is the natural frequency of the cylinder in the cross-flow direction. The amplitude of the cross-flow motion when the in-line motion of the cylinder is first eliminated (dashed curve) and then partially restrained by spring supports (dotted curve) is shown. In the latter case, the natural frequency for in-line vibration was also adjusted to be twice that of the cross-flow direction and this coincides with the frequency ratio between drag and lift. Two-dimensional VIV responses have also been predicted by direct numerical solutions of the Navier–Stokes equation coupled to the structure momentum equations (Karanth *et al.* 1995; Newman & Karniadakis 1995; Tamura *et al.* 1997). These coupled responses are often qualitatively different from the uncoupled responses.

The objective of this paper is to identify the principal mechanisms of coupled in-line and cross-flow motions of cable suspensions during VIV. One coupling mechanism originates

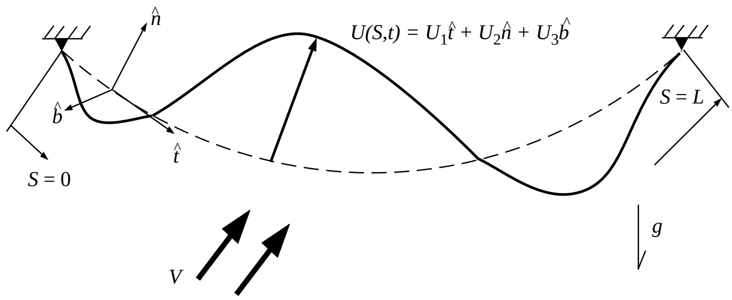

Figure 2. Schematic of cable of length L suspended between two level supports and with uniform fluid flow normal to the cable equilibrium plane.

from the cable alone and is controlled by the nonlinear stretching of the cable centerline. The second mechanism originates from a postulated relationship between fluid lift and drag. Both mechanisms follow from the following two-dimensional nonlinear model of the cable coupled to wake-oscillator models for fluctuating lift and drag.

2. GOVERNING EQUATIONS OF MOTION

The equations of motion for a sagged cable suspension are reviewed below together with phenomenological (wake-oscillator) models for fluid lift and drag. The cable momentum equations follow from the continuum model of an elastic cable derived by Perkins (1992) and extended by Newberry & Perkins (1997) for the case of fluid loading. Wake-oscillator models for the fluid forces are reviewed and are based on the lift model proposed by Skop & Balasubramanian (1997) and a drag model motivated by Currie & Turnbull (1987). A general wake-oscillator model for coupled lift and drag is also proposed.

2.1. Continuum Cable Model

A theoretical model for an elastic cable is reviewed that describes the dynamic response about a curved (sagged) equilibrium configuration. A uniform current is also assumed to flow perpendicular to the equilibrium plane as illustrated in Figure 2. The cable is modeled as a one-dimensional, homogeneous elastic continuum with negligible torsional, bending, and shear rigidities and obeying a linear stress–strain relationship for extension. The axial extension of the cable is described by the Lagrangian strain of the centerline.

Figure 2 depicts the cable in the equilibrium (dashed) and dynamic (solid) configurations where $\mathbf{U}(S,t) = U_1\hat{\mathbf{t}} + U_2\hat{\mathbf{n}} + U_3\hat{\mathbf{b}}$ denotes the three-dimensional displacement from equilibrium decomposed along the equilibrium tangential $\hat{\mathbf{t}}$, normal $\hat{\mathbf{n}}$, and binormal $\hat{\mathbf{b}}$ directions. Here, S denotes the equilibrium arc length coordinate and t denotes time. The normal coordinate $U_2(S,t)$ describes cross-flow response while the binormal coordinate $U_3(S,t)$ describes in-line response.

We shall focus on suspensions with small equilibrium sag defined by the condition $k = m_e gD/T^0 \ll 1$, where k is the nondimensional equilibrium curvature of the cable, m_e is the cable mass per unit length accounting for buoyancy, g is the gravitational acceleration, and T^0 is the equilibrium tension at the cable mid-span. Following Perkins (1992) and retaining terms in the equations of motion to order k^2 and using the quasistatic stretching assumption leads to the following nonlinear equations of cable motion:

$$[v_t^2 + v_l^2 h(t)]u_{2,ss} + kv_l^2 h(t) + F_L = \frac{m'}{m_e} Du_{2,tt}, \tag{1}$$

$$[v_t^2 + v_l^2 h(t)]u_{3,ss} + F_D = \frac{m'}{m_e} Du_{3,tt} \tag{2}$$

with the boundary conditions $u_j(0,t) = u_j(L/D,t) = 0,\ j = 2, 3$. In equations (1) and (2), the following nondimensional quantities are employed:

$$s = \frac{S}{D}, \qquad k = K^i D, \qquad \frac{v_t^2}{g} = \frac{T^0}{m_e Dg}, \qquad \frac{v_l^2}{g} = \frac{EA^i}{m_e Dg}, \quad \text{and} \quad u_j = \frac{U_j}{D}, \qquad j = 1, 2, 3,$$

where K^i is the equilibrium curvature of the cable. The axial stiffness of the cable cross-section is EA^i and m' denotes the cable mass/length including the added fluid mass $m' = (\rho_c + C_a \rho_f)A^i$. Here ρ_c is the cable density, ρ_f is the fluid density, C_a is the added mass coefficient, and A^i is the cable cross-sectional area.

In equations (1) and (2), F_L and F_D denote the fluid lift and drag, respectively, given by

$$F_L = \frac{\rho_f V^2 DC_L}{2m_e}, \qquad F_D = \frac{\rho_f V^2 D\tilde{C}_D}{2m_e}, \tag{3}$$

where C_L represents the fluctuating lift coefficient, and the drag coefficient $\tilde{C}_D = C_D - C_{Dm}$ is composed of both fluctuating C_D and mean C_{Dm} components. The nonlinear stretching of the cable centerline is described by the dynamic strain

$$h(t) = \frac{D}{L} \int_0^{L/D} \left\{ -ku_2 + \frac{1}{2}(u_{2,s}^2 + u_{3,s}^2) \right\} \mathrm{d}s. \tag{4}$$

A detailed derivation of this result can be found in Perkins (1992).

2.2. Discrete Model

A low-order cable model is proposed by assuming single-mode approximations for each coordinate $u_2(s,t)$ and $u_3(s,t)$ given by

$$u_2(s,t) = \alpha_i(t)V_{2i}(s), \qquad u_3(s,t) = \beta_j(t)V_{3j}(s), \tag{5}$$

where V_{2i} and V_{3j} are the (normalized) linear vibration mode shapes for the ith cross-flow and jth in-line modes, respectively (Perkins 1992). The validity of using these single mode approximations have been confirmed in Kim & Perkins (2000) by directly integrating equations (1) and (2) using space–time finite differencing together with wake-oscillator models for the fluctuating fluid lift and drag. Single-mode responses have also been considered in prior analytical studies and observed in experimental studies; for example, see Patrikalakis & Chryssostomidis (1985) and experimental studies cited therein.

Substitution of equation (5) into equations (1) and (2) and application of the Galerkin method leads to the following discrete model:

$$\ddot{\alpha}_i + 2\zeta_{2i}\omega_{2i}\dot{\alpha}_i + \omega_{2i}^2\alpha_i - A_1\alpha_i^2 - A_2\beta_j^2 + A_3\alpha_i^3 + A_4\alpha_i\beta_j^2 = \bar{\mu}\omega_{2i}^2 \int_0^{L/D} C_L V_{2i}\,\mathrm{d}s, \tag{6}$$

$$\ddot{\beta}_j + 2\zeta_{3j}\omega_{3j}\dot{\beta}_j + \omega_{3j}^2\beta_j - B_1\alpha_i\beta_j + B_2\alpha_i^2\beta_j + B_3\beta_j^3 = \frac{\bar{\mu}}{4}\omega_{3j}^2 \int_0^{L/D} \tilde{C}_D V_{3j}\,\mathrm{d}s \tag{7}$$

with

$$A_1 = \frac{3}{2}\left(\frac{m_e}{m'}\right)\frac{g v_l^2 r_i^2 \bar{V}_{2i}}{L v_t^4}, \qquad A_2 = \frac{g D \omega_{3j}^2 v_l^2 \bar{V}_{2i}}{2 L v_t^4}, \qquad A_3 = \left(\frac{m_e}{m'}\right)\frac{v_l^2 r_i^4}{2 L v_t^4},$$

$$A_4 = \frac{D \omega_{3j}^2 v_l^2 r_i^2}{2 L v_t^4}, \qquad B_1 = 2A_2, \qquad B_2 = A_4, \qquad B_3 = \left(\frac{m'}{m_e}\right)\frac{D^2 \omega_{3j}^4 v_l^2}{2 L v_t^4},$$

$$\bar{V}_{2i} = \int_0^{L/D} V_{2i}\, \mathrm{d}s, \qquad r_i^2 = \left(\frac{m'}{m_e}\right) D \omega_{2i}^2 - \frac{D g^2 \bar{V}_{2i}^2 v_l^2}{L v_t^4},$$

where modal damping terms (damping ratios ζ_{2i} and ζ_{3j}) have been introduced and the lock-in condition, $\omega_{2i} \cong \omega_s$ is assumed. Details of this derivation procedure can be found in Perkins (1992). In addition, $\bar{\mu} = (\rho_f D^2)/(8\pi^2 S_t^2 m')$ is the mass ratio of the displaced fluid to the cable mass. Here, ω_{2i} (ω_{3j}) denotes the natural frequency for the cross-flow (in-line) mode and ω_s is the vortex-shedding frequency (rad/s). The cross-flow and in-line motions of the cable are coupled through the quadratic and cubic nonlinearities due to cable stretching in equations (6) and (7). Note that the coefficients of the quadratic nonlinear terms vanish if V_{2i} is taken to be an antisymmetric mode.

The excitation frequency driving the cross-flow mode is the vortex-shedding frequency ω_s and that driving the in-line mode is $2\omega_s$ (Bishop & Hassan, 1964). Thus, simultaneous lock-in in both directions is possible if the natural frequencies are commensurable in a 1 : 2 ratio; i.e., $\omega_{3j} \cong 2\omega_{2i}$. This can be achieved by adjusting the cable sag so that the suspension is at one of several "cross-over points" as described by Irvine & Caughey (1974). This simultaneous lock-in may lead to larger two-dimensional motions of the cable and therefore represents a potential "worst-case" resonance.

2.3. Uncoupled Lift and Drag Model

The following uncoupled model for lift and drag will be referred to herein as Model A.

2.3.1. *Lift coefficient*

Following Skop & Balasubramanian (1997), the fluctuating lift coefficient is decomposed as

$$C_L(s,t) = Q(s,t) - \frac{2r}{\omega_s} u_{2,t}(s,t), \tag{8}$$

where r is a parameter to be evaluated from experimental data. The quantity $Q(s,t)$ is an excitation source, considered to develop from the spatial response of the cable and expressed as $Q(s,t) = q_i(t)V_{2i}(s)$. The temporal lift component q_i is governed by a Van der Pol equation,

$$\ddot{q}_i - \omega_{2i}\bar{G}\left(C_{L0}^2 - \frac{4}{\Gamma_i} q_i^2\right)\dot{q}_i + \omega_s^2 q_i = \omega_{2i}\bar{F}\dot{\alpha}_i, \tag{9}$$

where $\bar{G}$ and $\bar{F}$ are constants to be evaluated from experimental data, C_{L0} is the lift coefficient for a stationary cylinder, and Γ_i is a modal parameter defined as $\Gamma_i = (\int_0^{L/D} V_{2i}^2\, \mathrm{d}s)/(\int_0^{L/D} V_{2i}^4\, \mathrm{d}s)$. The second term on the right-hand side of equation (8) is called the stall term and provides self-limiting response for all system parameter values.

2.3.2. *Drag coefficient*

Currie & Turnbull (1987) proposed a Van-der-Pol-type wake-oscillator for the fluctuating drag which is similar to the lift wake-oscillator of Hartlen & Currie (1970). They modified the vibration frequency of the oscillator from that of Hartlen & Currie (1970) and introduced additional coupling terms in their model. In this study, we adopt a similar approach in adapting the wake-oscillator model in Skop & Balasubramanian (1997) for drag.

As described above, the drag coefficient $\tilde{C}_D$ is composed of the mean drag coefficient C_{Dm} and the fluctuating drag coefficient C_D. In this study, the mean drag is ignored by assuming that it does not affect the dynamics of the system and only provides a small static deflection in the downstream direction. The fluctuating drag component is

$$C_D(s,t) = P(s,t) + \frac{1}{\omega_{3j}} P_{,t}(s,t) - \frac{2r}{\omega_s} u_{3,t}(s,t), \tag{10}$$

where the excitation source $P(s,t)$ is expressed as $P(s,t) = p_j(t)V_{3j}(s)$, and $p_j(t)$ obeys the Van der Pol equation

$$\ddot{p}_j - \omega_{3j}\bar{V}\left(C_{D0}^2 - \frac{4}{\Gamma_j} p_j^2\right)\dot{p}_j + (2\omega_s)^2 p_j = \omega_{3j}\bar{W}\dot{\beta}_j. \tag{11}$$

Here, $\bar{V}$ and $\bar{W}$ are additional empirical constants to be determined, C_{D0} is the fluctuating drag coefficient for the stationary cylinder and $\Gamma_j = (\int_0^{L/D} V_{3j}^2 \, ds)/(\int_0^{L/D} V_{3j}^4 \, ds)$ is the modal parameter. This proposed model is used to describe the resonance region created by alternate vortex shedding. To predict the resonance region due to symmetric vortex shedding, another term must be added to the right-hand side of equation (11) as described in Currie & Turnbull (1987).

2.4. Coupled Lift and Drag Model

The lift and drag models above do not recognize the coupling between lift and drag force components that exists during the vortex-shedding process. To capture this coupling, a class of wake-oscillator models is proposed. Experimental measurements of in-line and cross-flow VIV show that the frequency of the in-line process (drag) is twice that of the cross-flow process (lift). This fact suggests that *quadratic* coupling between lift and drag may exist. To pursue this idea, equations (9) and (11) are now extended to include quadratic coupling terms:

$$\ddot{q}_i - \omega_{2i}\bar{G}[C_{L0}^2 - 4/\Gamma_i\, q_i^2]\,\dot{q}_i + \omega_s^2 q_i + \varepsilon(\kappa_1 q_i p_j + \kappa_2 \dot{q}_i \dot{p}_j + \kappa_3 \dot{q}_i p_j + \kappa_4 q_i \dot{p}_j) = \omega_{2i}\bar{F}\dot{\alpha}_i, \tag{12}$$

$$\ddot{p}_j - \omega_{3j}\bar{V}[C_{D0}^2 - 4/\Gamma_j p_j^2]\dot{p}_j + (2\omega_s)^2 p_j + \varepsilon(\kappa_5 q_i^2 + \kappa_6 \dot{q}_i^2 + \kappa_7 \dot{q}_i q_i) = \omega_{3j}\bar{W}\dot{\beta}_j, \tag{13}$$

where κ_n, $n = 1$–7, are empirical constants. This coupled lift and drag model will be referred to herein as Model B. The specific quadratic terms added above lead the periodic solutions, as discussed further in Section 4.2.

3. ANALYSIS OF PERIODIC MOTIONS

Periodic solutions describing steady oscillations during lock-in are sought to equations (6) and (7), either with the uncoupled fluid force model (9) and (11) (Model A), or with the coupled lift and drag model (12) and (13) (Model B). The method of multiple-scales (MMS) (Nayfeh & Mook 1979; Rahman & Burton 1989) is employed by introducing independent time scales and uniform expansions of the unknowns up to $\mathcal{O}(\varepsilon^3)$ in the new time scales:

$$t = \varepsilon^n T_0, \qquad n = 0, 1, 2, 3,$$

$$\alpha_i(t;\varepsilon) = \sum_{n=0}^{3} \varepsilon^n \alpha_n(T_0, T_1, T_2, T_3), \qquad q_i(t;\varepsilon) = \sum_{n=0}^{3} \varepsilon^n q_n(T_0, T_1, T_2, T_3), \tag{14}$$

$$\beta_j(t;\varepsilon) = \sum_{n=0}^{3} \varepsilon^n \beta_n(T_0, T_1, T_2, T_3), \qquad p_j(t;\varepsilon) = \sum_{n=0}^{3} \varepsilon^n p_n(T_0, T_1, T_2, T_3).$$

The resonance conditions, the damping coefficients, and the drag and lift parameters are also expanded as

$$\begin{aligned}
\omega_s &= \omega_{2i} + \varepsilon\sigma = \omega_{2i} + \varepsilon(\sigma_1 + \varepsilon\sigma_2 + \varepsilon^2\sigma_3),\\
\omega_{3j} &= 2\omega_{2i} + \varepsilon\rho = 2\omega_{2i} + \varepsilon(\rho_1 + \varepsilon\rho_2 + \varepsilon^2\rho_3),\\
2\zeta_{2i}\omega_{2i} &= 2\varepsilon S_G \mu\omega_{2i} = 2\varepsilon(k_1 + \varepsilon k_2 + \varepsilon^2 k_3),\\
2\zeta_{3j}\omega_{3j} &= 2\varepsilon S_G \mu\omega_{3j} = 2\varepsilon(h_1 + \varepsilon h_2 + \varepsilon^2 h_3),\\
C_{L0}^2\bar{G}\omega_{2i} &= \varepsilon C_{L0}^2 G\omega_{2i} = \varepsilon(G_1 + \varepsilon G_2 + \varepsilon^2 G_3),\\
C_{D0}^2\bar{V}\omega_{3j} &= \varepsilon C_{D0}^2 V\omega_{3j} = \varepsilon(V_1 + \varepsilon V_2 + \varepsilon^2 V_3),
\end{aligned} \tag{15}$$

where S_G is the reduced damping defined as $S_G = \zeta/\bar{\mu}$ (Griffin *et al.* 1982). Due to the symmetry of the cable, the damping ratios in both directions are assumed to be equal, i.e., $\zeta_{2i} = \zeta_{3j} = \zeta$. The first of these captures the fact that the vortex-shedding frequency is close to the natural frequency of the cross-flow mode. The frequency of the fluctuating drag is twice the vortex-shedding frequency (Bishop & Hassan 1964) and this can simultaneously lead to lock-in of the in-line mode provided that the natural frequency of the in-line mode is approximately twice that of the cross-flow mode. This condition, captured by the second equation in equation (15), is specifically selected to represent a worst-case scenario where lock-in may simultaneously exist for both cross-flow and in-line directions. The cable suspension can be tuned to achieve this 1 : 2 ratio of natural frequencies for cross-flow and in-line modes by adjusting the cable sag (or tension); refer to linear theory (Irvine & Caughey 1974). The remaining equations describe the ordering of the cable damping, lift, and drag parameters.

A standard procedure is used to find the periodic solutions to Models A and B and to access their local stability (Nayfeh & Mook 1979). Substituting equations (14) and (15) into equations (6) and (7), and either equations (9) and (11) (Model A) or equations (12) and (13) (Model B), and collecting terms of like powers in ε leads to a sequence of linear problems which are evaluated up to third order. By eliminating "secular terms" at each order, one obtains the eight first-order differential equations governing the amplitude and phase of each of the four unknowns (α_i, β_j, q_i, and p_j). The singular points of these amplitude/phase equations determine the steady-state periodic solutions of Models A or B. The (linear) stability of these periodic solutions can then be assessed from the local stability of the singular points.

4. RESULTS

An example cable suspension is selected to illustrate the major features of two-dimensional response. Table 1 lists the geometric and material parameters of the cable suspension and related fluid parameters. In Table 1, λ represents the cable parameter defined as $\lambda^2 = (v_l kL/(v_t D))^2$ (Irvine & Caughey 1974). Table 2 lists the empirical coefficients for the

TABLE 1
Cable suspension and fluid parameters for example in Section 4

Parameter	Value
Cable length (L)	4·38 m
Cable diameter (D)	0·0155 m
Cable material density (ρ_c)	4104·52 kg/m^3
Water density (ρ_f)	1025 kg/m^3
Reduced damping (S_G)	0·45455
Cable static tension (T^0)	175·74 N
Section modulus (EA)	$3{\cdot}1 \times 10^6$ N
Cable parameter (λ)	6π
Cross-flow natural frequency (ω_{2i})	58 rad/s
Added mass coefficient (C_a)	1·0
Strouhal number (St)	0·2

TABLE 2
Empirical coefficients for uncoupled lift and drag wake-oscillator models for example in Section 4

C_{L0}	0·28	C_{D0}	0·2
$\bar{G}$	0·3763	$\bar{F}$	1·0027
$\bar{V}$	0·3763	$\bar{W}$	0·10027

uncoupled lift and drag wake-oscillator models. The coefficients for the lift wake-oscillator follow those in Skop & Balasubramanian (1997). For the drag wake-oscillator, we select $\bar{V} = \bar{G}$ and $\bar{W} = \bar{F}/10$ which yields good agreement with published predictions (Currie & Turnbull 1987) of in-line response.

4.1. MODEL A: UNCOUPLED LIFT AND DRAG MODEL

We shall begin with results obtained using the uncoupled model for lift and drag (Model A) and evaluate both uncoupled and coupled cross-flow and in-line VIV. Any coupling in this instance derives solely from the geometric nonlinearities describing nonlinear stretching of the cable centerline.

4.1.1. *Uncoupled cross-flow and in-line VIV*

Consider first the simplest case of uncoupled response in the cross-flow and in-line directions. This follows from eliminating the geometrical coupling terms in equations (6) and (7) by setting $A_2 = A_4 = B_1 = B_2 = 0$. In addition, consider two predictions of the uncoupled responses based upon using: (i) the linearized cable model ($A_1 = A_3 = B_3 = 0$), and (ii) the geometrically nonlinear model ($A_1 \neq 0$, $A_3 \neq 0$, $B_3 \neq 0$).

The cross-flow response predicted from the linear cable model with the lift wake-oscillator is discussed first and provides a comparison with published results. Figure 3 shows the computed peak-to-peak amplitude for cross-flow vibration (normalized with respect to the cable diameter) as a function of the reduced damping parameter. To obtain this, the damping ratio ζ was varied and the maximum amplitude was calculated at each ζ. Also, the empirical coefficients $\bar{G}$ and $\bar{F}$ depend upon S_G; refer to Skop & Balasubramanian

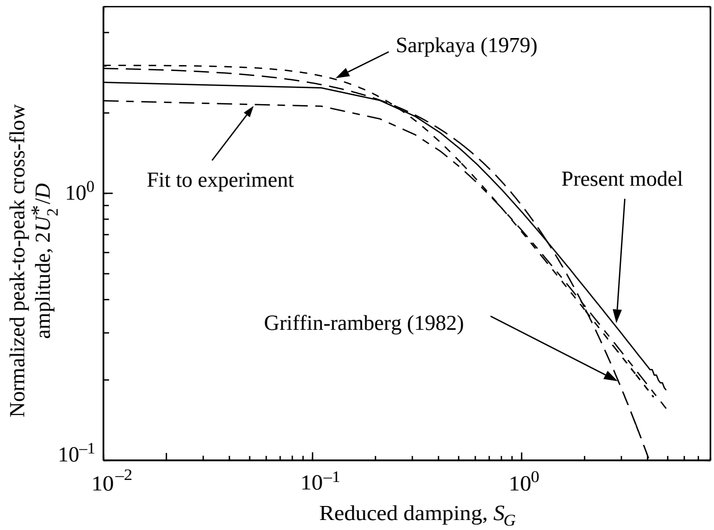

Figure 3. Computed peak-to-peak amplitude for cross-flow response of linearized cable model as a function of reduced damping, $S_G = \zeta/\bar{\mu}$. The quantity U_2^* is the amplitude at an antinode.

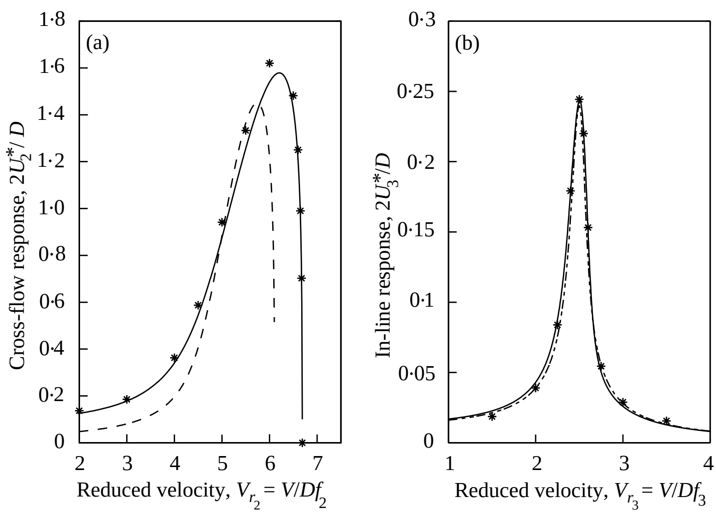

Figure 4. Vibration amplitude versus reduced velocity for (a) cross-flow and (b) in-line vibration. $U_j^*, j = 2, 3$ is the amplitude at an antinode and $f_j, j = 2, 3$ is the natural frequency of the cable (Hz) in the cross-flow and in-line directions, respectively: —, perturbation analysis; $*$, numerical results; – – –, results of Hartlen & Currie (1970) in (a); ---, Currie & Turnbull (1987) in (b).

(1997). Linearized cable model prediction (solid curve) compares well with the least-squares fit to the experimental results (Skop & Balasubramanian 1997) and analytical results (dashed curves) for taut strings and cylinders; see Blevins (1990) and reference to Sarpkaya (1979) and Griffin & Ramberg (1982) therein. These predictions and experiments highlight the self-limiting nature of the responses that leads to a maximum peak-to-peak amplitude of about two cable diameters.

Figure 4 illustrates the computed amplitudes for both cross-flow and in-line vibrations as functions of the reduced fluid velocity in the neighborhood of lock-in. The solid curves

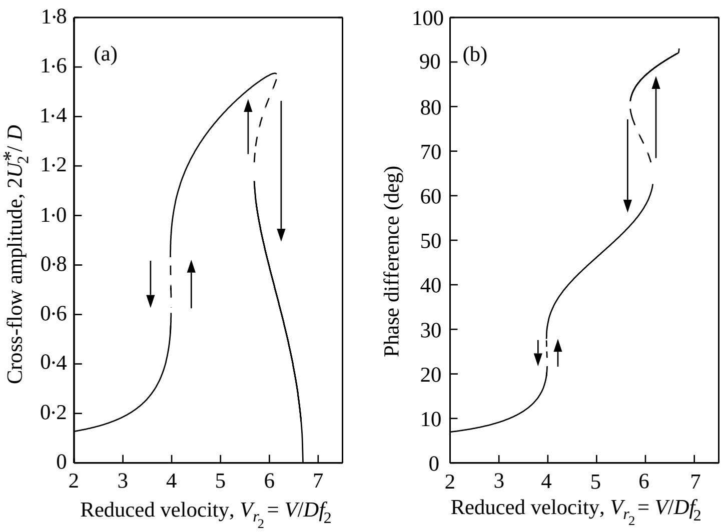

Figure 5. Cross-flow response computed from uncoupled nonlinear cable model: (a) peak-to-peak vibration amplitude; (b) phase difference between lift and cross-flow displacement. Solid (dashed) curves denote stable (unstable) periodic solutions.

represent the amplitudes predicted by the perturbation analysis and these compare favorably with results obtained using direct numerical integration of equations (6) and (7) with equations (9) and (11); see asterisks. Moreover, the results agree with published predictions for cross-flow (Hartlen & Currie 1970) and in-line (Currie & Turnbull 1987) vibration; see dashed curves. Note that the maximum amplitude for cross-flow and in-line vibration occur near $V_r \approx 6$ and 2·5, respectively. The lock-in ranges for cross-flow and in-line vibration are $3 < V_{r_2} < 6{\cdot}5$ and $1{\cdot}5 < V_{r_3} < 3{\cdot}5$, respectively. In short, the wake-oscillator models used with the linearized cable models capture the basic characteristics of VIV well-known in the literature.

Geometric nonlinearities describing the stretching (but no coupling) of a sagged cable are now introduced to the cable model. The nonlinearities in general produce multiple periodic motions and hysteresis as seen in the following results. In all figures that follow, solid (dashed) curves denote stable (unstable) periodic solutions obtained from the perturbation analysis.

Figure 5 illustrates (a) the computed vibration amplitude for cross-flow response and (b) the phase angle between the lift and the cross-flow displacement. The results shown in Figure 5(a) exhibit a softening behavior at small amplitudes, where the quadratic nonlinearity [term associated with A_1 in equation (6)] dominates and a hardening behavior at large amplitudes where the cubic nonlinearity dominates [term associated with A_3 in equation (6)]. These nonlinearities create multiple stable periodic solutions (distinguishable as either large or small amplitude responses) with associated hysteresis as the reduced velocity increases or decreases. Jumps occur at the boundaries of the lock-in region over which the phase angle changes by 90°, as shown in Figure 5(b). Hysteresis has been reported in several experiments (Brika & Laneville 1993; Fujarra *et al.* 1998) and the predicted cable response shows a qualitative resemblance to these experimental results. Thus, hysteresis can be caused by structural nonlinearities alone (as well as by other nonlinear mechanisms).

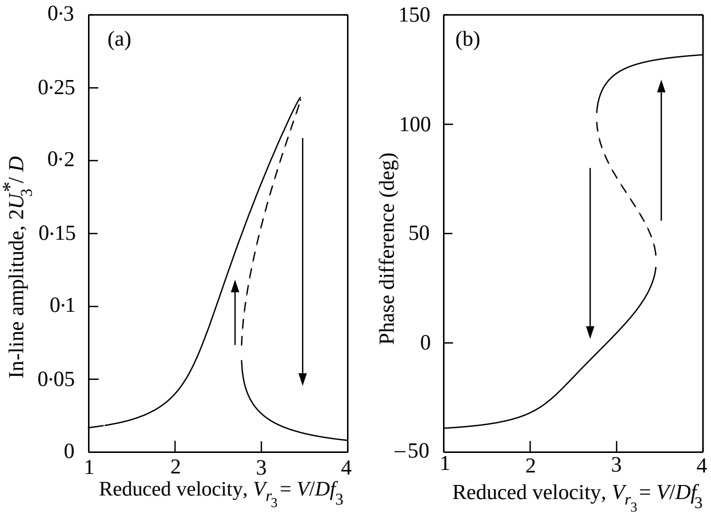

Figure 6. In-line response computed from uncoupled nonlinear cable model: (a) peak-to-peak vibration amplitude; (b) phase difference between drag and in-line displacement. Solid (dashed) curves denote stable (unstable) periodic solutions.

Similar conclusions can be drawn from Figure 6 which shows the amplitude and phase for in-line response. Note that the observable hardening behavior originates from the cubic nonlinearity [term associated with B_3 in equation (7)] due to cable stretching. Note also that the maximum amplitude is approximately the same as for the linear cable model [Figure 4(b)] but the lock-in range is now increased by nearly a factor of two.

4.1.2. *Coupled cross-flow and in-line VIV*

Nonplanar cable responses result from the coupling between cross-flow and in-line motions due to two major mechanisms: (i) structural nonlinearities, and (ii) coupled lift and drag. Here, attention is focused first on the coupling solely from the structural nonlinearities.

Structural coupling of the in-line and cross-flow coordinates originates through the quadratic and cubic nonlinearities associated with cable stretching; refer to terms with coefficients A_2, A_4, B_1, and B_2 in equations (6) and (7). Figure 7 illustrates the computed cross-flow and in-line amplitudes as a function of the reduced velocity for the coupled cable model. Note that a nonplanar solution branch ($U_2 \neq 0$ and $U_3 \neq 0$) bifurcates from the planar solution branch ($U_3 = 0$). The terms in equations (6) and (7) with coefficients A_2, A_4, B_1, and B_2 become secular when the natural frequencies are close to the internal resonance condition $\omega_{3j} \cong 2\omega_{2i}$ and this leads to strong modal interactions. Examination of the differential equations (6) and (7) with equations (9) and (11) reveals that planar response (trivial in-line motion $\beta_j = 0$) is always a possible (steady-state) solution. Nonplanar (coupled cross-flow and in-line) solutions exist when the cross-flow response exceeds a critical amplitude.

The perturbation analysis also reveals that the out-of-plane response is largely controlled by the 1 : 2 internal resonance of the cross-flow and in-line modes rather than the fluctuating fluid drag. Note also that the predicted periodic solutions of Figure 7 are always unstable (except for a very small region near $V_{r_2} \sim 6$ in Figure 7(a)). This fact is confirmed by results obtained by the direct numerical integration of equations (6) and (7) with equations (9) and

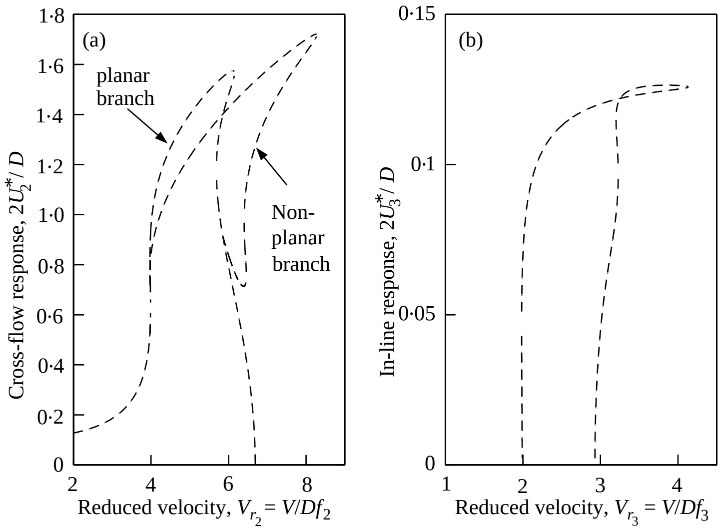

Figure 7. Coupled (nonplanar) response of nonlinear cable model. Amplitude (peak-to-peak) of periodic solutions plotted versus reduced velocity: (a) cross-flow response; (b) in-line response. Solid (dashed) curves represent the amplitude of stable (unstable) periodic response.

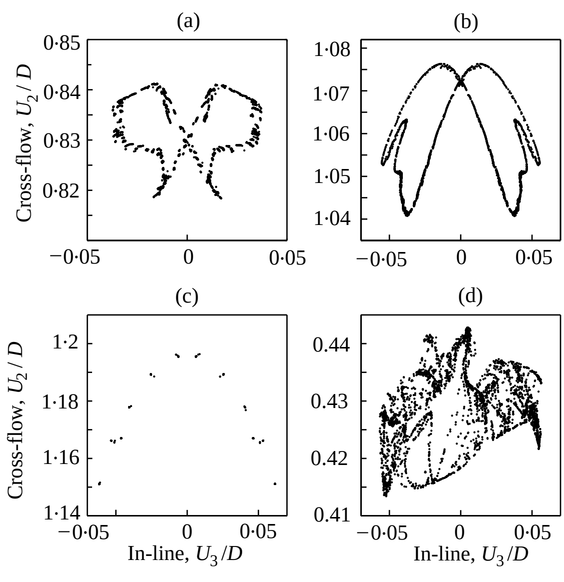

Figure 8. Poincaré map for nonplanar response of nonlinear cable model at $V_{r_2} = 4$, 5, and 6. The map is created by sampling α_i and β_j every cycle of the cross-flow motion when $\dot{\alpha}_i = 0$. (a) $V_{r_2} = 4$; (b) $V_{r_2} = 5$; (c) $V_{r_2} = 6$, large amplitude (d) $V_{r_2} = 6$, small amplitude.

(11) as illustrated in the Poincaré maps of Figure 8. For instance, at $V_{r_2} = 4$ and 5, the maps illustrate quasiperiodic motions having well-defined symmetry with respect to the equilibrium plane of the cable. At $V_{r_2} = 6$, two attractors coexist with the larger amplitude response being a periodic motion [Figure 8(c)] and the smaller amplitude response being a likely chaotic motion [Figure 8(d)].

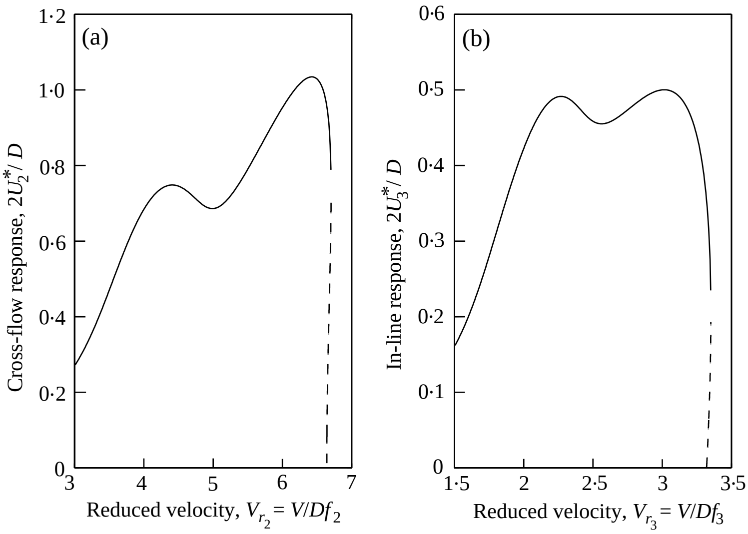

Figure 9. Predicted response of the cable suspension with 1 : 2 internal resonance, using proposed coupled lift/drag model: (a) cross-flow response; (b) in-line response. The amplitudes of stable periodic solutions (—) and unstable solutions (- - -) are shown.

4.2. Model B: Coupled Lift and Drag Model

The wake oscillator model of Section 2.4 is proposed as one means to recognize the coupling of lift and drag during the vortex-shedding process. Quadratic coupling terms are introduced, noting that the fluctuating drag occurs at a frequency twice that of lift.

A first-order perturbation analysis is carried out on Model B and reveals that, of all possible quadratic coupling terms, only those shown in equations (12) and (13) affect the periodic solutions (to first order). Moreover, the terms with constants κ_1 and κ_2 have the same qualitative effect on this dynamical system. Thus, without loss of generality, the coupling terms that affect periodic response can be parameterized by four coefficients; namely,

$$\Upsilon_1 = \left(\frac{\kappa_1}{4\omega_{2i}} + \frac{\kappa_2\omega_{2i}}{2}\right), \quad \Upsilon_2 = \left(-\frac{\kappa_3}{2} + \frac{\kappa_4}{4}\right), \quad \Upsilon_3 = \left(-\frac{\kappa_5}{8\omega_{2i}} + \frac{\kappa_6\omega_{2i}}{8}\right), \quad \Upsilon_4 = \left(\frac{\kappa_7}{8}\right).$$

We now return to the previous example suspension and re-evaluate the predicted response with the added fluid coupling terms above. To this end, we select $\Upsilon_1 = -30$, $\Upsilon_2 = 175$, $\Upsilon_3 = -1400$ and $\Upsilon_4 = 1600$ based upon comparison of the computed response with published experimental measurements (on flexibly mounted cylinders) as reported in Wu (1989) and Moe *et al.* (1994).

Figure 9 illustrates the predicted cable responses for Model B (with the linearized cable model). These responses are qualitatively different from the results of Model A. In particular, note that two relative maxima exist for the in-line and cross-flow amplitudes within the lock-in region and that the in-line response is substantially greater than that predicted by Model A for uncoupled lift/drag.

Consider next a qualitative comparison between the in-line and cross-flow VIV previously measured on a spring supported rigid cylinder (Wu 1989) with that predicted for a flexible cable. The justification for making such a comparison is that the near-wake properties along the cable are similar to those of a rigid cylinder for comparable vibration

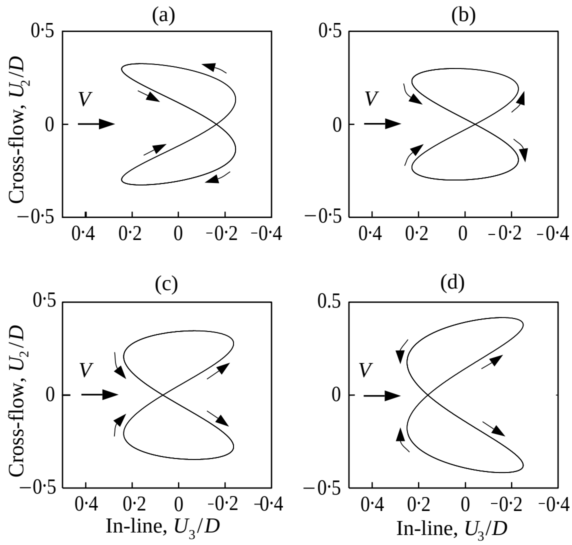

Figure 10. Computed two-dimensional motion of the cable cross-section at $s = (11L)/(24D)$ using the new coupled wake-oscillator model. Results reported for (a) $V_{r_2} = 4{\cdot}5$, (b) 5·0, (c) 5·5 and (d) 6·0, where $\omega_{3j}/\omega_{2i} = 2$.

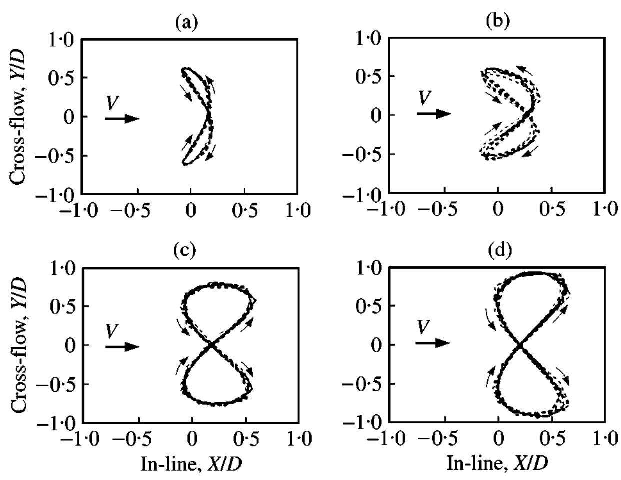

Figure 11. Measured two-dimensional motion of the cylinder cross-section when both cross-flow and in-line directions are spring supported. Results reported for (a) $V_r = 4{\cdot}9508$, (b) 5·6911, (c) 6·3860, and (d) 6·7116. Reproduced from Wu (1989).

amplitudes and frequencies (Ramberg & Griffin 1974, 1976). The predicted amplitudes of the cross-flow and in-line motions of the cable during lock-in are illustrated in Figure 9 over the reduced velocity range that includes lock-in in both directions. The results of Figure 9(a) for cross-flow response exhibit the two relative maxima as reported by Moe *et al.* (1994) for a flexibly mounted cylinder; refer to Figure 1.

The resulting nonplanar motion of the cable cross-section is shown in Figure 10 for four values of the reduced fluid velocity within the lock-in range. The trajectory of the cable is a figure of eight that bends towards the upstream direction at lower reduced velocities and then towards the downstream direction at higher reduced velocities within the lock-in region. These predicted results are also in good qualitative agreement with the experimental measurements reported in Wu (1989) and Moe *et al.* (1994) for spring-supported cylinders. For example, Figure 11 illustrates the measured nonplanar trace of the cylinder cross-section for a comparable range of reduced velocity as reproduced from Wu (1989). In this example, the natural frequency of the in-line direction is twice that of cross-flow direction, i.e., $\omega_x/\omega_y = 2$. It is emphasized that while this comparison between the response of a flexible cable and a flexibly supported cylinder shows remarkably similar features, a quantitative validation of the results of this analytical study would require a dedicated experiment on cable suspensions.

5. CONCLUSIONS

A model for an elastic cable with small sag subject to a uniform cross-flow is presented which captures the quadratic and cubic nonlinearities describing nonlinear cable stretching. Fluid forces acting on the cable are modeled using (phenomenological) wake-oscillator models for lift and drag. A discrete four-degree-of-freedom model is developed for studying the periodic motions representing planar and nonplanar vortex-induced vibrations. A perturbation analysis is reviewed that provides the periodic solutions and their stability within the lock-in region. Both planar (pure cross-flow and pure in-line) motions and nonplanar (coupled in-line and cross-flow) motions are evaluated.

Pure cross-flow and pure in-line responses predicted by the linearized cable models capture the basic characteristics of VIV and provide good agreement with published results. However, qualitatively different behaviors are predicted when the cable geometric nonlinearities are included. Multiple stable periodic solutions coexist within the lock-in regimes for both cross-flow and in-line vibrations and both exhibit hysteresis.

Coupled cross-flow and in-line motions may originate from two coupling mechanisms: structural nonlinearities and coupled lift/drag. The structural nonlinearities alone produce qualitatively different dynamic characteristics compared to the limiting uncoupled models including nonplanar and aperiodic motions. Both planar and non-planar responses coexist with nonplanar responses bifurcating from the planar responses. A coupled lift and drag model is proposed in the form of a two-dimensional wake-oscillator with quadratic coupling terms. The proposed model captures the salient features of the nonplanar responses that have been observed in prior experiments on spring supported cylinders.

ACKNOWLEDGMENT

The authors wish to acknowledge the U.S. Office of Naval Research for support of this research.

REFERENCES

ALEXANDER, C. M. 1981 The complex vibrations and implied drag of a long oceanographic wire in cross-flow. *Ocean Engineering* **8,** 379–406.

BISHOP, R. E. D. & HASSAN, A. Y. 1964 The lift and drag forces on a circular cylinder oscillating in a flowing fluid. *Proceedings of the Royal Society of London*, *Series* A **277,** 51–75.

BLACKBURN, H. & HENDERSON, R. 1996 Lock-in behavior in simulated vortex-induced vibration. *Experimental Thermal and Fluid Science* **12,** 184–189.

BLEVINS, R. D. 1990 *Flow-Induced Vibration.* New York: Van Nostrand Reinhold.

BLEVINS, R. D. & BURTON, T. E. 1976 Fluid forces induced by vortex shedding. *ASME*, *Journal of Fluids Engineering* **98,** 19–26.

BRIKA, D. & LANEVILLE, A. 1993 Vortex-induced vibrations of a long flexible circular cylinder. *Journal of Fluid Mechanics* **250,** 481–508.

CURRIE, I. G. & TURNBULL, D. H. 1987 Streamwise oscillations of cylinders near the critical Reynolds number. *Journal of Fluids and Structures* **1,** 185–196.

FUJARRA, A. C., PESCE, C. P. & PARRA, P. P. H. 1998 Vortex induced vibrations experiments on a flexible cylinder. *Proceedings of the Eighth International Offshore and Polar Engineering Conference*, Vol. **III**, pp. 393–399. Montreal, Canada.

GOSWAMI, I., SCANLAN, R. H. & JONES, N. P. 1993 Vortex-induced vibration of circular cylinders. II: New model. *ASME*, *Journal of Engineering Mechanics* **119,** 2288–2302.

GRIFFIN, O. M. & RAMBERG, S. E. 1982 Some recent studies of vortex shedding with application to marine tubulars and risers. *ASME Journal of Energy Resources Technology* **104,** 2–13.

GRIFFIN, O. M., VANDIVER, J. K., SKOP, R. A. & MEGGITT, D. J. 1982 The strumming vibrations of marine cables. *Ocean Science and Engineering* **7,** 461–498.

HARTLEN, R. T. & CURRIE, I. G. 1970 Lift-oscillator model of vortex-induced vibration. *ASCE Journal of the Engineering Mechanics* **96,** 577–591.

IRVINE, H. M. & CAUGHEY, T. K. 1974 The linear theory of free vibrations of a suspended cable. *Proceedings of the Royal Society of London*, *Series* A **341,** 299–315.

IWAN, W. D. & BLEVINS, R. D. 1974 A model for vortex induced oscillation of structures. *Journal of Applied Mechanics* **41,** 581–586.

KARANTH, D., RANKIN, G. W. & SRIDHAR, K. 1995 Computational study of flow past a cylinder with combined in-line and transverse oscillation. *Computational mechanics* **16,** 1–10.

KENNEDY, M. & VANDIVER, J. K. 1979 A random vibration model for cable strumming prediction. *ASCE Civil Engineering in the Oceans* **IV,** 273–292.

KIM, W.-J. & PERKINS, N. C. 2000 Nonlinear two dimensional vortex induced vibration of an elastic cable. *Proceedings of ETCE/OMAE Joint Conference*, New Orleans, LA, U.S.A., Paper OMAE2000-8010.

LU, X. Y. & DALTON, C. 1996 Calculation of the timing of vortex formation from an oscillating cylinder. *Journal of Fluids and Structures* **10,** 527–541.

MOE, G., HOLDEN, K. & YTTERVOLL, P. O. 1994 Motion of spring supported cylinders in subcritical and critical water flows. *Proceedings of the Fourth International Offshore and Polar Engineering Conference*, Vol. III, pp. 468–475, Osaka, Japan.

NAUDASCHER, E. 1987 Flow-induced streamwise vibrations of structures. *Journal of Fluids and Structures* **1,** 265–298.

NAYFEH, A. H. & MOOK, D. T. 1979 *Nonlinear Oscillations*. New York: John Wiley & Sons.

NEWBERRY, B. L. & PERKINS, N. C. 1997 Investigation of resonant tensioning in submerged cables subjected to lateral excitation. *International Journal of Offshore and Polar Engineering* **7,** 48–53.

NEWMAN, D. J. & KARNIADAKIS, G. E. 1995 Direct numerical simulations of flow over a flexible cable. *Proceedings of the Sixth International Conference Flow-Induced Vibration*, London, U.K. pp. 193–203. Rotterdam: Balkema.

PANTAZOPOULOS, M. S. 1994 Vortex-induced vibration parameters: critical review. *Proceedings International Conference on Offshore Mechanics and Arctic Engineering*, Vol. 1, pp. 199–255, Houston, TX, U.S.A.

PARKINSON, G. 1989 Phenomena and modeling of flow-induced vibrations of bluff bodies. *Progress in Aerospace Sciences* **26,** 169–224.

PATRIKALAKIS, N. M. & CHRYSSOSTOMIDIS, C. 1985 Vortex-induced response of a flexible cylinder in a constant current. *ASME Journal of Energy Resources Technology* **107,** 244–249.

PERKINS, N. C. 1992 Modal interactions in the non-linear response of elastic cables under parametric/external excitation. *International Journal of Non-Linear Mechanics* **27,** 233–250.

RAHMAN, Z. & BURTON, T. D. 1989 On higher order methods of multiple scales in non-linear oscillations — periodic steady state response. *Journal of Sound and Vibration* **133,** 369–379.

RAMBERG, S. E. & GRIFFIN, O. M. 1974 Vortex formation in the wake of a vibrating, flexible cable. *ASME Journal of Fluids Engineering* **96,** 317–322.

RAMBERG, S. E. & GRIFFIN, O. M. 1976 Velocity correlation and vortex spacing in the wake of a vibrating cable. *ASME Journal of Fluids Engineering* **98,** 10–18.

SARPKAYA, T. 1979 Vortex-induced oscillations: a selective review. *Journal of Applied Mechanics* **46,** 241–258.

SKOP, R. A. & BALASUBRAMANIAN, S. 1997 A new twist on an old model for vortex-excited vibrations. *Journal of Fluids and Structures* **11,** 395–412.

SKOP, R. A. & GRIFFIN, O. M. 1973 A model for the vortex-excited resonant response of bluff cylinders. *Journal of Sound and Vibration* **27,** 225–233.

STAUBLI, T. 1983 Calculation of the vibration of an elastically mounted cylinder using experimental data from forced oscillation. *ASME Journal of Fluids Engineering* **105,** 225–229.

TAMURA, T., HAYAKAWA, A. & OKADA, R. 1997 Numerical study on aeroelastic behavior of a circular cylinder with two degrees of freedom. *ASME Fourth International Symposium on Fluid-Structure Interactions*, *Aeroelasticity*, *Flow-Induced Vibration and Noise*, Vol. 1, pp. 217–226, Dallas, TX, U.S.A.

WU, Z. J. 1989 Current induced vibrations of a flexible cylinder. Ph.D. thesis, The University of Trondheim, Norway.